RSC Advances

ROYAL SOCIETY
OF CHEMISTRY

www.rsc.org/advances

Optimization of the zinc oxide electron transport layer in P3HT:PC61BM based organic solar cells by annealing and yttrium doping

Sayantan Das and T. L. Alford[*]

Department of Chemistry and Biochemistry and School for Engineering of Matter, Transport and Energy Arizona State University, Tempe, Arizona 85287, USA

Abstract

Zinc-oxide and yttrium-doped ZnO films were fabricated by a sol–gel processing technique and were incorporated as an electron transport layer in inverted organic solar cells (with an active layer comprising a blend of P_3HT and $PC_{61}BM$). First, the annealing conditions for the pure sol-gel ZnO layers were optimized. An interesting observation was that the anneal temperature of the ZnO layer significantly influenced the overall organic solar cells performance. Annealing the ZnO film at temperatures of ~150 °C provided the highest device performance. Physical and surface properties of these ZnO films were examined by X-ray diffraction, atomic force microscopy and UV-vis transmittance measurements. Utilizing the optimized annealing conditions, we further fabricated high-efficiency organic solar cells by doping yttrium in the zinc-oxide (YZO) electron transport layers. The efficiency of YZO based devices was improved by 30% when compared to that of the undoped zinc oxide based devices.

Keywords: photovoltaics, heterojunctions, zinc oxide, yttrium doping, interface engineering

*Corresponding author: tel.: 001 480 965 7471
E-mail address: TA@asu.edu

1.   INTRODUCTION

Until today the civilized society is almost entirely dependent upon fossil fuels for nearly every part of its existence. However, it becomes quiet unpleasant to realize that at some point the fossil fuels are going to be extinct or become too expensive for an average person to use it [1]. Moreover, the uncontrolled use of fossil fuels has also increased carbon dioxide (CO_2) emissions causing increased average global temperature [1]. This has led to the increasing demand for cheap, renewable and clean energy source across the globe and organic solar cells (OSCs) are one of the promising solutions [2-5]. In OSCs, a blend of regioregular poly(3-hexylthiophene) (P_3HT) and the fullerene derivative [6,6]-phenyl-C61 butyric acid methyl ester ($PC_{61}BM$) forms a phase-separated (BHJ) nanostructure which offers a large interfacial area for efficient exciton dissociation and is also the most widely researched donor and acceptor materials [5]. Recently, Guo *et al* fabricated and characterized P_3HT:$PC_{61}BM$ based OSCs under AM0 (stands for air mass zero) illumination for testing its potential use in space applications [6]. These materials have the potential to be manufactured cheaply as flexible large area sheets with low-cost materials at low temperature using roll-to-roll processes [7-11]. However, in order to become marketable and start to make an impact in power generation, several obstacles must first be overcome such as lower efficiencies than commercially available Si solar cells and relatively short OSC lifetimes due to degradation [12-16].

In case of OSC devices the energy level alignment at the interfaces between each layer plays a crucial role in determining the short circuit current (J_{sc}), open circuit voltage (V_{oc}), and fill factor (FF) [17]. For example, in case of OSCs, the presence of non-ohmic contacts in between electrode and the organic layers may result in a lower V_{oc}, while application of interfacial layers resulted in enhanced V_{oc} [17-20]. Furthermore, interfacial layers helps in the

improvement of the charge collection efficiency and decrease in the interfacial contact resistance which leads to smaller series resistance (R_s) and larger shunt resistance (R_{sh}) [17, 21, 22].

In the inverted structure of OSCs, a high work function metal like silver is used as a hole collecting electrode, while the n-type metal oxides such as SnO_2, TiO_2 and ZnO are used as the electron transport layer (ETL) [23-25]. Among the metal oxides, ZnO serves as an excellent ETL due to its high electron mobility, good transparency, availability, non-toxicity, and hole blocking properties [25]. Pure ZnO has been widely used in organic/polymer based solar cells, perovskite based solar cells and dye sensitized solar cells [26-28]

Recently, in order to increase the device performance of inverted solar cells, several groups have studied the use of metal doped n-type buffer layers. Metal doping is an efficient technique to modify the optical and electrical properties of ZnO layers [29]. Dopant atoms such as Al, Ga, In, Sn, Ta and Y have been explored as potential n-type dopants for ZnO; because, they can replace the Zn sites in the ZnO crystal and generate free electrons [30-35].

In this article, we report the effects of ZnO processing temperature on the photovoltaic properties of inverted solar cells with the structure of $ITO/ZnO/P_3HT:PC_{61}BM/MoO_x/Ag/Al$. The best device performance is observed with the ZnO layers annealed at 150 °C despite the fact that higher temperatures leads to improvement in thin film crystallinity and electron mobility [36]. We further investigated the use of yttrium as a doping impurity to enhance the electron transport properties in the ZnO films. The efficiency of solar cells has further been improved by using optimized concentration of yttrium ions in the ZnO (YZO) film enabling them to become excellent electron transport layers.

2.   EXPERIMENTAL SECTION

2.1. Preparation of zinc oxide and yttrium-doped zinc oxide precursor solution:

ZnO and yttrium doped ZnO precursor solution was prepared by dissolving 0.5 M zinc acetate dihydrate $((Zn(CH_3CO_2)_2.2H_2O)$ in N,N-dimethylformamide (99.8%, Sigma–Aldrich) with monoethanolamine (MEA) as chelating agent (stabilizer). $YCl_3.6H_2O$ in different amounts was added into the solution and the mixture solution was then stirred on a hot plate at 60 °C for about 1 h until the solution changed to a clear transparent solution. This solution was then aged for a day before further use.

2.2 Device Fabrication:
All devices in this work were prepared on 40Ω sq^{-1} ITO coated glass substrates. The substrates were cleaned in sequential ultrasonic baths of acetone, methanol, and isopropanol, followed by ultraviolet ozone (UVO) treatment for 10 min. The ZnO/YZO precursor solution was spin coated at 3000 rpm for 60s onto cleaned patterned ITO substrate. The precursor solutions was then subjected to heat treatment at various temperatures for an hour (discussed later) on a hot plate in order to convert the precursor materials into ZnO/YZO. Immediately prior to the active layer ($P_3HT:PC_{61}BM$) deposition, ultraviolet ozone (UVO) treatment for 2 min was performed on the ZnO/YZO layers to remove organic residues that might be present on the ZnO/YZO surface. Photoactive layers were then spin-coated from $P_3HT:PC_{61}BM$ blends dissolved in 1, 2- dichlorobenzene (DCB) in 1:1 weight ratio at 600 rpm for 1 min. The photoactive layer (150 nm) was then dried at 150 °C for 15 min. In addition, after spin-coating, the photoactive layer was left inside the N_2 filled glove box for 24 h to increase P_3HT ordering. The device structure was completed by evaporating MoOx (10nm)/Ag (10 nm)/Al (70 nm).

2.3. Characterization of the ZnO layer: X-ray diffraction (XRD) patterns were recorded at room temperature using a Philips X'PertPro diffractometer equipped with a Cu Kα radiation (λ = 1.54056 Å). A working voltage of 45kV was employed with a filament current of 40mA. Surface morphology of the ZnO layers on ITO was acquired by using atomic force microscopy (AFM). The optical transmittance of glass/ITO/ZnO and ITO/YZO thin films were measured using Ocean Optics double channel spectrometer (model DS200) in a wavelength range of 300–800 nm.

2.4. Device Characterization: Current density-voltage (*J-V*) measurements were performed under simulated AM 1.5 global solar irradiation (100 mW/cm^2) using a xenon-lamp solar simulator (Spectra Physics, Oriel Instruments, USA). The light source was calibrated with a standard Si photodiode reference cell (Hamamatsu Photonics, Japan) prior to measurement

3. RESULTS AND DISCUSSION

3.1 Effect of annealing temperature on ZnO thin films and corresponding solar cell performance

Figure 1 demonstrates the electronic structure of the inverted solar cells. In this inverted structure, electrons are transferred from PC$_{61}$BM to the ITO/ZnO cathode and holes in P$_3$HT towards the MoOx/Ag/Al anode. Organic stabilizers like monoethanolamine (MEA) used during ZnO film formation needs to be removed before the deposition of the active layer (P$_3$HT: PC$_{61}$BM) to enhance the electronic contact between the ETL and the active layer as well as that among ZnO grains [37]. Earlier reports suggest that a short UVO treatment can effectively remove the organic capping agents and improve electronic coupling among the ZnO grains thus improving solar cell efficiency [37-39]. Nevertheless, prolonged UVO treatment reduces the

number of free electrons in the conduction band by filling the oxygen atom vacancies with an adverse effect on the device performance [40].

Table 1 summarized the data derived from the J–V characteristics of the solar cell devices fabricated using solution processed ZnO layer annealed at different temperatures. By inspecting the device properties we were able to observe effect of annealing the ZnO layer after spin coating. The OSCs utilizing ZnO ETL annealed at 50 °C exhibited a PCE of 1.28% with a V_{oc} of 0.59 V, a J_{sc} of 7.78 mA cm^{-2}, and a fill factor (FF) of 27.8%. The OSCs fabricated with ZnO layers annealed at 150 °C showed significant improvement in the PCE by ~70% to 2.18% (V_{oc} = 0.60 V, J_{sc} = 8.72 mA cm^{-2}, and FF = 41.7%). Higher temperature annealing treatments of ZnO layer however showed continuous depreciation in cell performance, and the PCE became 1.00% for the cells with ZnO annealed at 450 °C.

In solar cell devices, R_{sh} and R_s are important parameters and often used to quantify the quality of the films and their interfaces. In an ideal situation, the series resistance is close to zero while the shunt resistance approaches a large value. The R_s depends on the resistivity of the different layers in the OSC and electrodes while the R_{sh} depends on recombination of charge carriers occurring near the different interfacial layers and at the electrode [21]. We thus hypothesize here that the excessive heat treatment can modify the surface properties of the ZnO layer, affecting the performance of the cells. At first instance it is expected that a higher crystallinity will lead to better electron transport and reduced R_s. In fact the R_s value of the device decreases when ZnO layer is annealed from 50 °C to 150 °C and the PCE increased. However, further increasing the annealing temperature from 150 °C to 450 °C results in a drop in the R_{sh}, indicating higher leakage current resulted from higher surface roughness of ZnO ETLs. Table 1 suggests that only optimum thermal treatment of the ITO covered ZnO layer is beneficial

for the cell performance whereas excessive annealing of the ZnO layer deteriorates the device performance.

To investigate the effect of different annealing temperature on the surface roughness of the ZnO thin films, samples annealed at 150 °C and 450 °C are investigated by AFM. Figure 2(a) and (b) are AFM images of the single layer ZnO film on glass substrates prepared by annealing at 150 °C and 450 °C, respectively. The ZnO film annealed at 450 °C is comparatively rougher with a root-mean square (rms) roughness of 5.7 nm than the film annealed at 150 °C (rms of 2.2 nm). In organic solar cell structures the smoother surface is expected to facilitate a uniform interfacial contact between the ETLs and active layers, thus increasing the electron collection efficiency.

The structure of the ZnO was verified by spin coating the precursor solution multiple times on glass substrates followed by annealing on a hot plate for 150 °C, 300 °C and 450 °C. The structure of the ZnO films were evaluated using x-ray diffraction (XRD) method. The precursor solution was spin coated on glass substrate six times followed by annealing at different temperatures for 1 hour. Figure 3 shows the XRD patterns of ZnO thin films on glass substrates and confirms that samples annealed at 150 °C had amorphous structures, whereas samples annealed at 300 °C and 450 °C shows a pronounced ZnO peak at 34.4° (2θ) corresponding to the (002) reflection of the hexagonal cubic wurtzite structure (JCPDS card No. 79-2205) [41]. The *c*-axis lattice constant of ZnO films was found to be 0.52 nm. The optical transmittance of glass/ITO/ZnO films annealed at different temperatures shows good optical transmittance in the visible region. Figure 4 shows no significant difference in transmittance values regardless of the annealing temperature except the one annealed at 450 °C which might be due to degradation of ITO [42].

3.2   Effect of yttrium doping of ZnO thin films on the efficiency of OSCs

It has been reported previously that the resistivity of ZnO films further decreases after doping with yttrium ions; however, excessive doping leads to increase in the resistivity of the films [33, 43]. At low doping concentrations Y^{3+} ion substitutes the Zn^{2+} lattice sites as donors, resulting in an increased number of charged carriers, but beyond a critical limit carrier concentration saturates and resistivity starts to rise due to enhanced scattering from the dopant ions [44]. Thus, to investigate the effects of doping in zinc oxide for the inverted OSCs, different concentrations of the n-type dopant (Y^{3+}) was added to the zinc oxide precursor solution and spin coated on top of ITO layer, followed by annealing at 150 °C on a hot plate inside the glove box. Fig. 5 illustrates the UV-Vis absorption spectra of various YZO thin films and indicates that the transmittance spectra have no significant difference regardless of the amount of yttrium added. All the ZnO/YZO films have good optical transmittance in the visible region. It might be because the YZO films are very thin and could be considered as completely transparent. Thus the introduction of various amounts of yttrium in ZnO layers has no significant effect to the UV-Vis absorption spectra.

The J–V characteristics of the $P_3HT:PC_{61}BM$ based OSCs fabricated using ETLs of ZnO and YZO are shown in Fig. 6 and the data derived from it is illustrated in Table 2. As reported earlier the OSC device with ZnO exhibits a J_{sc} of 8.72 mA cm^{-2}, V_{oc} of 0.60 V, FF of 41.7% and PCE of 2.18%. The OSC incorporating an ETL composed of 0.5 at.% Y-doped ZnO exhibits an improved photovoltaic response with J_{sc} of 9.19 mA cm^{-2}, Voc of 0.59 V, FF of 49.2% and thus a PCE of 2.66%. The efficiency of the inverted organic solar cell fabricated with 1.0 at. % Y-doped ZnO exhibited the best photovoltaic performance among all the devices, with PCE of 2.85%, J_{sc} of 9.81 mA cm^{-2}, V_{oc} of 0.59 V and FF of 49.3%. Further increase in the yttrium

RSC Advances

concentration beyond 1 at. % leads to slight depreciation of the device performance as evident from their PCE values.

It is observed that increasing the Y-concentration from 0 to 1.0 at. % leads to improvement in the solar cell performance by ~30%. The increase in fill factor from 41.7% to 49.3% has also been attributed to improved electron–hole mobility in the device [45]. This significant enhancement of the PCE in YZO based devices could be attributed to the improved mobility of the YZO ETLs as compared to the ZnO ETL, thus increasing the J_{sc}. Moreover, the R_s value of all the YZO based devices are significantly lower than the ZnO based devices resulting in increased PCE values. These results indicate that power conversion efficiency of the ZnO based devices can be improved through Y-doping of the ZnO layer, however; it is also noted that exceeding the Y doping beyond 1.0 at. % leads to the decrease in the device performance.

4. CONCLUSIONS

In this study, the performance of ZnO ETLs in ITO/ZnO/P$_3$HT:PC$_{61}$BM/MoOx/Ag/Al structures with optimized annealing conditions was reported through characterization of the surface morphology, thin film crystallinity, and optical and device properties. It was found that the proper ZnO annealing condition plays a dominant role in determining the device performance for sol–gel processed ZnO. Based on these findings, an approach to fabricate and optimize high-efficiency P$_3$HT: PC$_{61}$BM solar cells was determined by using yttrium-doped zinc oxide as the ETL. Our results in this work suggest that such a doping approach can provide a brilliant solution for the enhancement of PCE in organic solar cells, however optimum doping conditions should be maintained to observe best device performance. This study showed that by doping an

optimized amount of yttrium into zinc oxide layer resulted in a 30% enhancement of PCE. This implies that interfacial engineering is a promising approach for manipulating the efficiency of organic/polymer based solar cells in low-cost roll-to-roll manufacturing.

References

[1]   Krebs, F. C; Espinosa, N.; Hösel, M.; Søndergaard, R. R.; Jørgensen, M.; 25th anniversary article: Rise to power-OPV based solar parks. Adv. Mater. **2014**, *26*, 29–39.

[2]   Brabec, C. J.; Sariciftci, N. S.; Hummelen, C.; Plastic solar cells. Adv. Funct. Mater. **2001**, *11*, 15–26.

[3]   Spanggaard, H.; Krebs, F. C.; A brief history of the development to of organic and polymeric photovoltaics. Sol. Energy Mater. Sol. Cells **2004,** *83*, 125–146.

[4]   Hoppe, H.; Sariciftci, N. S.; Organic solar cells: an overview. J. Mater. Res. **2004**, *19*, 1924–1945.

[5]   Dang, M. T.; Hirsch, L.; Wantz, G.; P3HT:PCBM, Best seller in polymer photovoltaic research, Advanced Materials 23 (2011)3597-3602.

[6]   Guo, S.; Brandt, C.; Andreev, T.; Metwalli, E.; Wang, W.; Pelich, J.; Muller-Buschbaum, P.; First Step into Space: Performance and morphological evolution of P3HT:PCBM bulk heterojunction solar cells under AM0 illumination ACS Appl. Mater. Interfaces **2014**, *6*, 17902−17910.

[7]   Krebs, F. C.; Fabrication and processing of polymer solar cells: a review of printing and coating technique. Sol. Energy Mater. Sol. Cells **2009**, *93*, 394–412.

[8]   Krebs, F. C.; All solution roll-to-roll processed polymer solar cells free from indium-tin-oxide and vacuum coating steps. Org. Electron. **2009**, *10*, 761–768.

[9]   Kim, J. Y.; Lee, K.; Coates, N. E.; Moses, D.; Nguyen, T.-Q.; Dante, M.; Heeger, A. J.; Efficient tandem polymer solar cells fabricated by all-solution processing. Science **2007**, *317*, 222-225.

[10]   Dang, M. T.; Hirsch, L.; Wantz, G.; P3HT:PCBM, Best seller in polymer photovoltaic research. Adv. Mater. **2011** *23*, 3597-3602.

[11]   Chen, L. M.; Hong, Z.; Li, G.; Yang, Y.; Recent progress in polymer solar cells: manipulation of polymer: fullerene morphology and the formation of efficient inverted polymer solar cells. Adv. Mater. **2009**, *21*, 1434–1449.

[12]   Schaffer, C. J.; Palumbiny, C. M..; Niedermeier, M. A.; Jendrzejewski, C.; Santoro, G.; Roth, S. V.; Muller-Buschbaum, P.; A direct evidence of morphological degradation on a nanometer scale in polymer solar cells. Adv.Mater. **2013**, *25*, 6760-6764.

[13]   Vongsaysy, U.; Bassani, D. M.; Servant, L.; Pavageau, B.; Wantz, G.; Aziz, H.; Formulation strategies for optimizing the morphology of polymeric bulk heterojunction organic solar cells: a brief review. J. Photonics Energy **2014**, *4*, 040998–041019

[14]   Dutta, P.; Xie, Y.; Kumar, M.; Rathi, M.; Ahrenkiel, P.; Galipeau, D.; Qiao, Q.; Bommisetty, V.; Connecting physical properties of spin-casting solvents with morphology, nanoscale charge transport, and device performance of poly(3-hexylthiophene):phenyl-C_{61}-butyric acid methyl ester bulk heterojunction solar cells. J. Photonics Energy **2011**, *1* 011124–011140.

[15] Vongsaysy, U.; Pavageau, B.; Wantz, G.; Bassani, D. M.; Servant, L.; Aziz, H.; Guiding the selection of processing additives for increasing the efficiencies of bulk heterojunction polymeric solar cells. Adv. Energy Mater. **2014**, *4*, 1300752-1300760.

[16] Jorgensen, M.; Normann, K.; Krebs, F. C.; Stability/degradation of polymer solar cells. Sol. Energy Mater. Sol. Cells, **2008**, *92*, 686-714.

[17] Steim, R.; Kogler, F. R.; Brabec, C. J.; Interface materials for organic solar cells. J. Mater. Chem., **2010**, *20*, 2499–2512.

[18] Xin, H.; Subramaniyan, S.; Kwon, T.-W.; Shoaee, S.; Durrant, J. R.; Jenekhe, S. A.; Enhanced open circuit voltage and efficiency of donor-acceptor copolymer solar cells by using indene-C60 bisadduct. Chem. Mater. **2012**, *24*, 1995−2001.

[19] Chen, H.-Y.; Hou, J.; Zhang, S.; Liang, Y.; Yang, G.; Yang, Y.; Yu, L.; Wu, Y.; Li, G.; Polymer solar cells with enhanced open-circuit voltage and efficiency. Nat. Photonics. **2009**, *3*, 649-653.

[20] Lee, J.-Y.; Kim, S.-H.; Song, I.-S.; Moon, D.-K.; Efficient donor–acceptor type polymer semiconductors with well-balanced energy levels and enhanced open circuit voltage properties for use in organic photovoltaics. J. Mater. Chem. **2011**, *21*, 16480–16487.

[21] Ma, H.; Yip, H. –L.; Huang, F.; Jen, A. K.-Y.; Interface engineering for organic electronics. Adv. Funct. Mater. **2010**, *20*, 1371–1388.

[22] Chen, L.-M.; Xu, Z.; Hong, Z.; Yang, Y.; Interface investigation and engineering-achieving high performance polymer photovoltaic devices. J. Mater. Chem. **2010**, *20*, 2575–2598.

[23] Bob, B.; Song, T.-B.; Chen, C.-C.; Xu, Z.; Yang, Y.; Nanoscale dispersions of gelled SnO_2: Material properties and device applications, Chem. Mater. **2013**, *25*, 4725−4730.

[24] Lin, Z; Jiang, C.; Zhu, C.; Zhang, Z, Development of inverted organic solar cells with TiO_2 interface layer by using low-temperature atomic layer deposition. ACS Appl. Mater. Interfaces, **2013**, *5*, 713−718.

[25] Sun, Y.; Seo, J. H.; Takacs, C. J. Seifter, J.; Heeger, A. J.;Inverted polymer solar cells integrated with a low-temperature-annealed sol-gel derived ZnO film as an electron transport layer. Adv. Mater. **2011**, *23*, 1679-1683.

[26] Ka, Y.; Lee, E.; Park, S. Y.; Seo, J.; Kwon, D.-G.; Lee, H. H.; Park, Y.; Kim, Y. S.; Kim, C.; Effect of annealing temperature of aqueous solution-processed ZnO electron-selective layers on inverted polymer solar cells. Org. Electron **2013**, *14*, 100-104.

[27] Liu, D.; Kelly, T. L.; Perovskite solar cells with a planar heterojunction structure prepared using room-temperature solution processing techniques. Nat. Photonics **2014**, *8*, 133-138.

[28] Sarkar, K.; Braden, E. V.; Pogorzalek, S.; Yu, S.; Roth, S. V.; Muller-Buschbaum, P.; Monitoring structural dynamics of in situ spray-deposited zinc oxide films for application in dye-sensitized solar cells. ChemSusChem **2014**, *7*, 2140–2147

[29] Minami, T.; Transparent conducting oxide semiconductors for transparent electrodes. Semicond. Sci. Technol. **2005**, *20*, S35–S44.

[30] Minami, T.; Nanto, H.; Takata, S.; Highly conductive and transparent aluminum doped zinc oxide thin films prepared by RF magnetron sputtering. Jpn. J. Appl. Phys. **1984**, *23*, L280-L282.

[31] Cheng, Y.; Cao, L.; He, G.; Yao, G.; Song, X.; Sun, Z.; Preparation, microstructure and photoelectrical properties of tantalum-doped zinc oxide transparent conducting films, J. Alloys Compd. **2014**, *608*, 85–89

[32] Major, S.; Chopra, K. L.; Indium doped zinc oxide films as transparent electrodes for solar cells. Sol. Energy Mater. **1988**, 17, 319-327

[33] Kaur, R.; Singh, A. V.; Mehra, R. A.; Structural, electrical and optical properties of sol–gel derived yttrium doped ZnO films. Phys. Stat. Sol. (a) **2005**, *202*, 1053–1059.

[34] Chandra, R. D.; Rao, M.; Zhang, K.; Prabhakar, R. R.; Shi, C.; Zhang, J.; Mhaisalkar, S. G.; Mathews, N.; Tuning electrical properties in amorphous zinc tin oxide thin films for solution processed electronics. ACS Appl. Mater. Interfaces **2014**, *6*, 773−777.

[35] Minami, T.; Sato, H.; Nanto, H.; Takata, S.; Group III impurity doped zinc oxide thin films prepared by RF magnetron sputtering. Jpn. J. Appl. Phys. **1985**, *24*, L781-L784.

[36] Lee, J.-H.; Ko, K.-H.; Park, B.-O.; Electrical and optical properties of ZnO transparent conducting films by the sol–gel method. J. Cryst. Growth, **2003**, *247*, 119–125.

[37] Cho, J. M.; Kwak, S.-W.; Aqoma, H.; Kim, J. W.; Shin, W. S.; Moon, S.-J.; Jang, S.-Y.; Jo, J.; Effects of ultraviolet–ozone treatment on organic-stabilized ZnO nanoparticle-based electron transporting layers in inverted polymer solar cells. Org. Electron. **2014**, *15*, 1942–1950

[38] Kato, Y.; Jung, M.-C.; Lee, M. V.; Qi, Y.; Electrical and optical properties of transparent flexible electrodes: effects of UV ozone and oxygen plasma treatments, Org. Electron. **2014**, *15*, 721–728.

[39] Ip, K.; Gila, B. P.; Onstine, A. H.; Lambers, E. S.; Heo, Y. W.; Baik, K. H.; Norton, D. P.; Pearton, S. J.; Kim, S.; LaRoche, J. R.; Ren, F.; Improved Pt/Au and W/Pt/Au Schottky contacts on n-type ZnO using ozone cleaning. Appl. Phys. Lett. **2004**, *84*, 5133–5135.

[40] Bao, Q.; Liu, X.; Xia, Y.; Gao, F.; Kauffmann, L.-D.; Margeat, O.; Ackermann, J.; Fahlman, M.; Effects of ultraviolet soaking on surface electronic structures of solution

RSC Advances Accepted Manuscript

processed ZnO nanoparticle films in polymer solar cells. J. Mater. Chem. A, **2014**, *2*, 17676–17682.

[41] Klug, H. P.; Alexander, L. E.; X-ray Diffraction Procedures for Polycrystalline and Amorphous Materials. Wiley, New York, 1974

[42] Jiang, C.; Lunt, R. R.; Duxbury, P. M.; Zhang, P. P.; High-performance inverted solar cells with a controlled ZnO buffer layer. RSC Adv., **2014**, *4*, 3604-3610.

[43] Yu, Q.; Fu, W.; Yu, C.; Yang, H.; Wei, R.; Sui, Y.; Liu, S.; Liu, Z.; Li, M.; Wang, G.; Shao, C.; Liu, Y.; Zou, G.; Structural, electrical and optical properties of yttrium-doped ZnO thin films prepared by sol–gel method. J. Phys. D: Appl. Phys. **2007**, *40*, 5592–5597.

[44] Han, X.; Han, K.; Tao, M.; Low resistivity yttrium-doped zinc oxide by electrochemical deposition. J. Electrochem. Soc. **2010**, *157*, H593-H597.

[45] Weickert, J.; Dunbar, R. B.; Hesse, H. C.; Wiedemann, W.; Schmidt-Mende, L.; Nanostructured organic and hybrid solar cells. Adv. Mater. **2011**, *23*, 1810–1828.

List of Tables

TABLE 1 Device parameters of ZnO based inverted organic solar cells under illumination
(average of five devices)

ZnO anneal Temperature (^{O}C)	V_{oc}(V)	J_{sc}(mA/cm^2)	FF(%)	R_{sh}(Ω.cm^2)	R_s(Ω.cm^2)	PCE(%)
50	0.59	7.78	27.8	130	39	1.28
150	0.60	8.72	41.7	510	13	2.18
300	0.60	8.76	32.9	150	28	1.73
450	0.48	6.64	31.4	92	9	1.00

TABLE 2 Device parameters of Y doped ZnO based inverted organic solar cells under illumination(average of five devices)

ETL	V_{oc}(V)	J_{sc}(mA/cm^2)	FF(%)	R_{sh}(Ω.cm^2)	R_s(Ω.cm^2)	PCE(%)
ZnO	0.60	8.72	41.7	510	13	2.18
0.5%YZO	0.59	9.19	49.2	283	7	2.66
1.0%YZO	0.59	9.81	49.3	254	6	2.85
1.5%YZO	0.60	8.98	51.5	334	9	2.77
2.0%YZO	0.60	8.99	50.3	258	6	2.71

Figure Captions (Color Online)

FIG. 1   Energy level diagram of different components of the OSC devices

FIG. 2   4×4 μm^2 tapping mode AFM images of single layer ZnO film on glass substrates annealed at (a) 150 °C and (b) 450 °C, respectively.

FIG. 3   XRD patterns of ZnO on glass substrate prepared by annealing at (a) 150 °C (b) 300 °C and (c) 450 °C.

FIG. 4   Optical transmission spectra of sol-gel prepared single layer ZnO on ITO coated glass substrates annealed at different temperatures

FIG. 5   Optical transmission spectra of sol-gel prepared zinc oxide and yttrium doped zinc oxide layers on ITO coated glass substrates

FIG. 6   Current density-voltage (J–V) characteristics of the ZnO and Y doped ZnO based OPV devices under illumination.
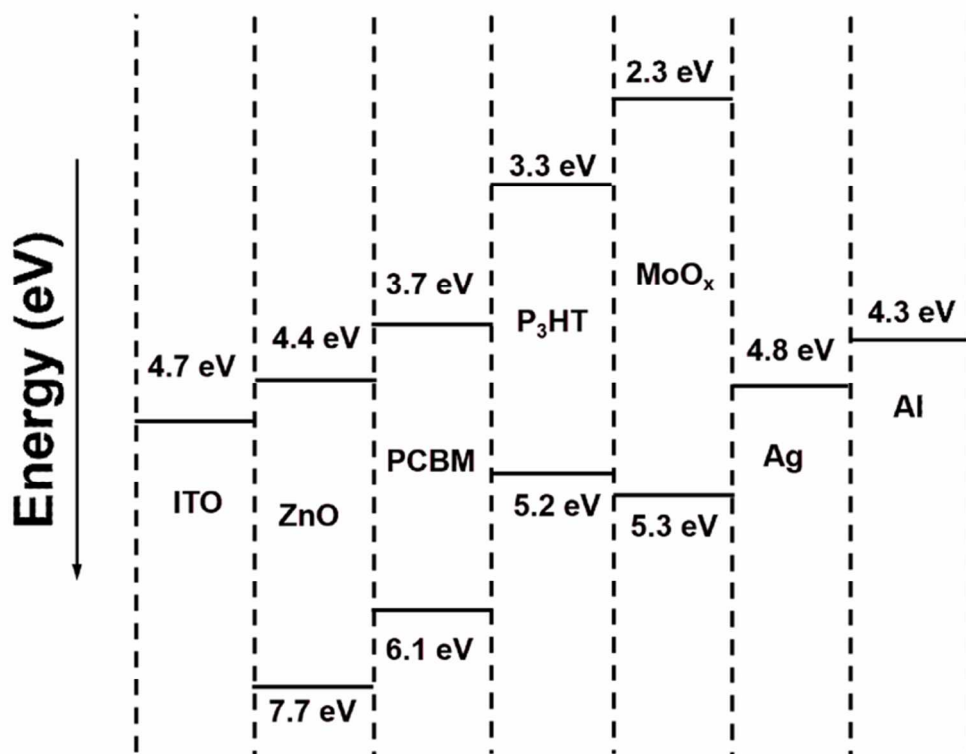
66x52mm (300 x 300 DPI)
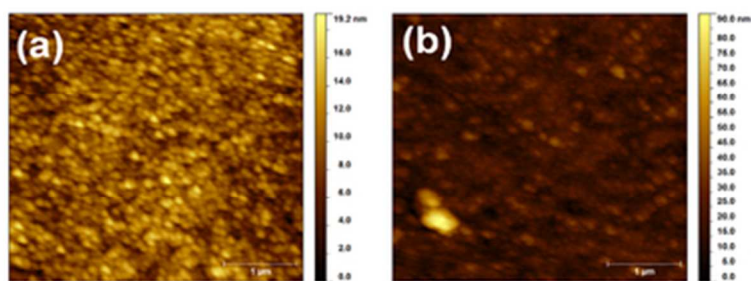
33x13mm (300 x 300 DPI)
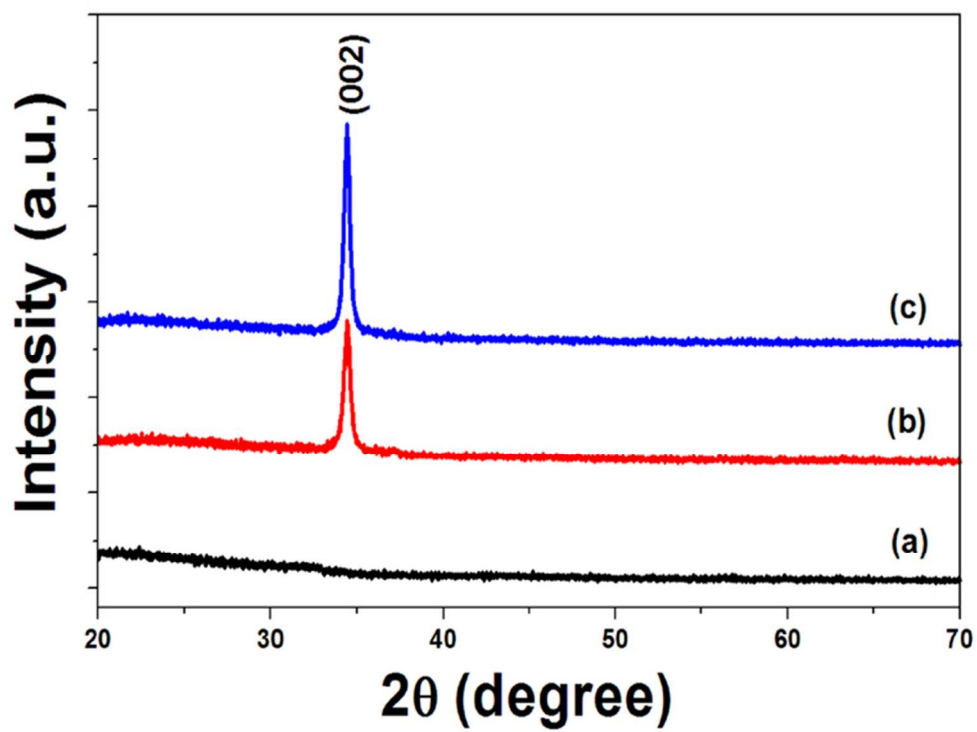
66x52mm (300 x 300 DPI)
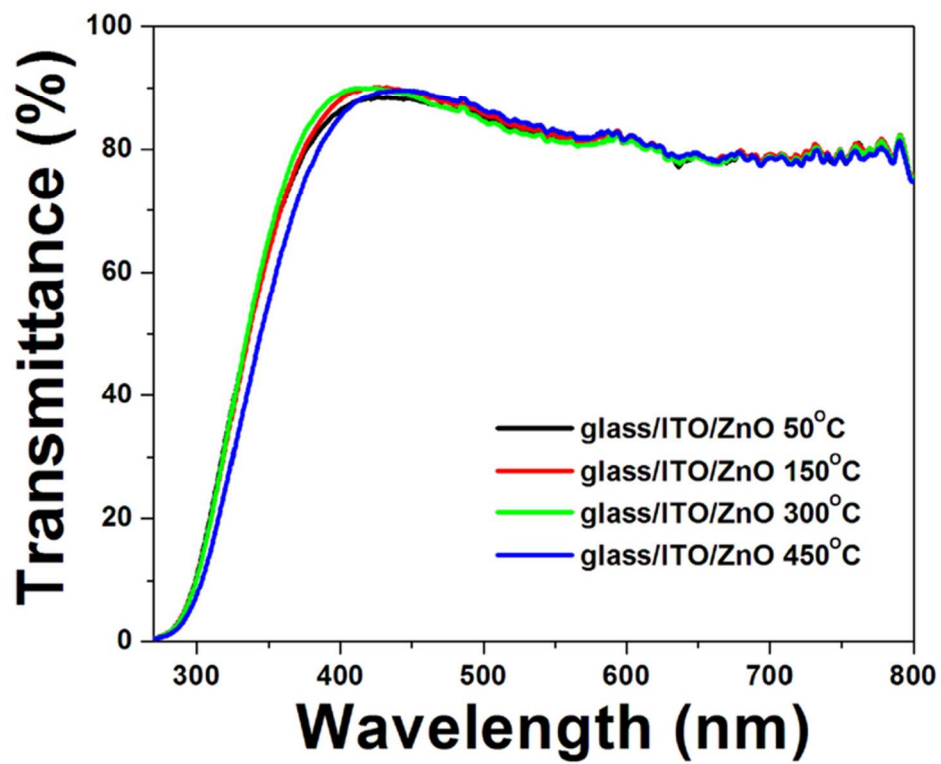
66x52mm (300 x 300 DPI)
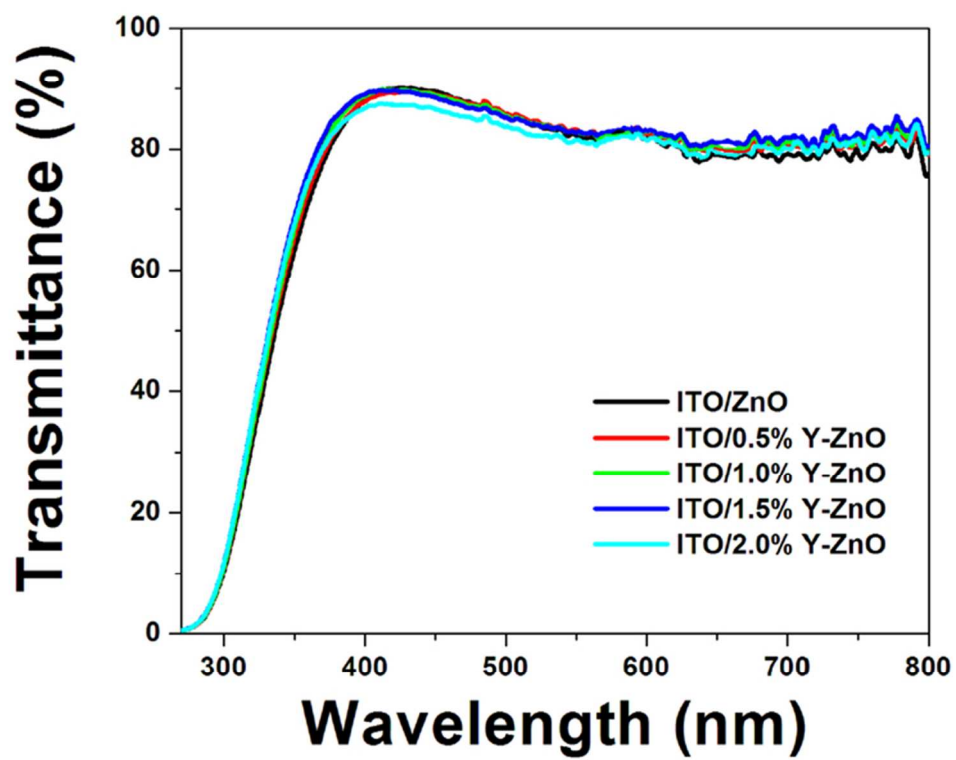
66x52mm (300 x 300 DPI)
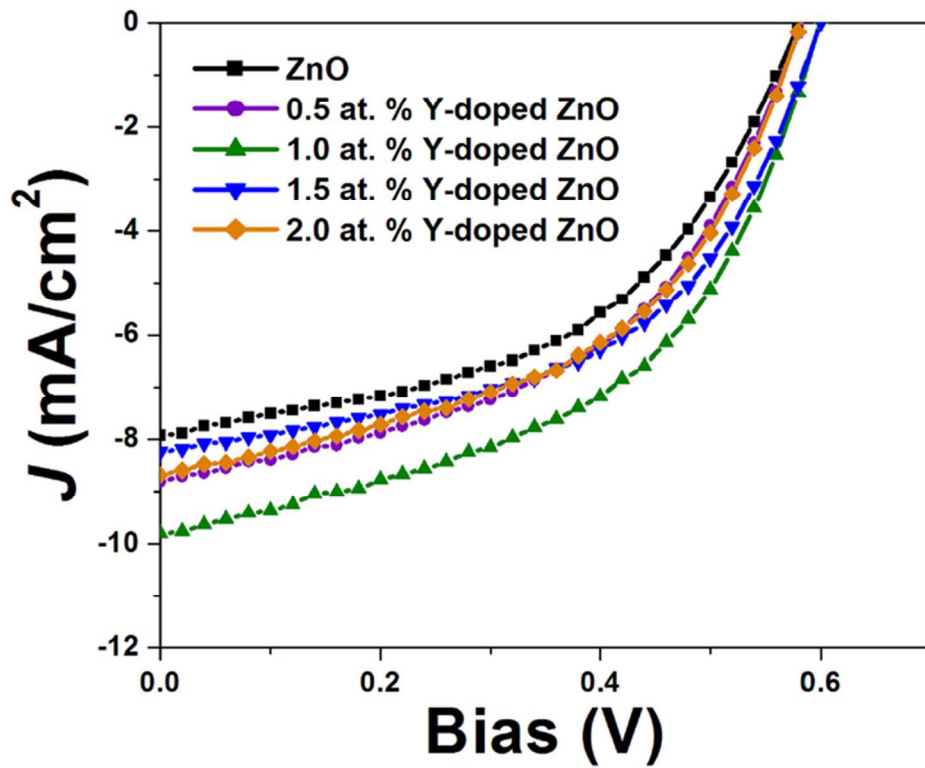
66x52mm (300 x 300 DPI)

Graphical Abstract

Yttrium-doped zinc oxide were utilized as efficient electron-transport layer in $P_3HT:PC_{61}BM$ based solar cells.